A Posteriori Dual-Mixed (Hybrid) Adaptive Finite Element Error Control for Lamé and Stokes Equations

A Posteriori Dual-Mixed (Hybrid) Finite Element Error Control

Carsten Carstensen[1], Paola Causin[2], Riccardo Sacco[3]

[1] Department of Mathematics, Humboldt-Universität zu Berlin, Unter den Linden 6, D-10099 Berlin, Germany. E-Mail: `cc@math.hu-berlin.de`
[2] INRIA Rocquencourt, B.P.105 Domaine de Voluceau, F-78153 Le Chesnay Cedex, Rocquencourt, France. E-Mail: `paola.causin@inria.fr`
[3] MOX - Modeling and Scientific Computing, Dipartimento di Matematica "F. Brioschi", Politecnico di Milano, via Bonardi 9, 20133 Milano, Italy.
E-Mail: `riccardo.sacco@mate.polimi.it`

Abstract A unified and robust mathematical model for compressible and incompressible linear elasticity can be obtained by rephrasing the Herrmann formulation within the Hellinger-Reissner principle. This quasi-optimally converging extension of PEERS (Plane Elasticity Element with Reduced Symmetry) is called Dual-Mixed Hybrid formulation (DMH). Explicit residual-based a posteriori error estimates for DMH are introduced and are mathematically shown to be locking-free, reliable, and efficient. The estimator serves as a refinement indicator in an adaptive algorithm for effective automatic mesh generation. Numerical evidence supports that the adaptive scheme leads to optimal convergence for Lamé and Stokes benchmark problems with singularities.

1 Introduction and motivation

It is well known that for nearly incompressible and incompressible materials, i.e. for a value of the Poisson ratio near or equal to 0.5, finite element computations based on a standard displacement formulation fail due to the onset of the locking phenomenon (see [11] for numerical evidence). A valid alternative to locking-affected methods is represented by dual-mixed formulations, that provide mathematical models capable of treating under

an unified framework both compressible and incompressible linear elasticity problems (see [3,18]). However, the quasi-optimal convergence rate of such methods can be unfavorably degraded, for example, by the presence of singularities in the computational domain. In such an event, the convergence performance can be improved by resorting to a robust mesh-refinining algorithm for an efficient automatic mesh-design. A list of contributions proposing and analyzing robust and effective adaptive finite element methods in compressible, nearly incompressible and pure incompressible solid and fluid mechanics includes references [4,10,11,13,12,17,23,24].

In the sequel, we will deal with a dual-mixed formulation obtained by rephrasing the Herrmann approach [20] within the Hellinger-Reissner principle. This quasi-optimally converging extension of PEERS (Plane Elasticity Element with Reduced Symmetry) is called Dual-Mixed Hybrid formulation (DMH) and in the case of isotropic materials reads: *Given the linear functionals $G(\tau)$ and $F(v)$, find $(\sigma, u, \gamma, p) \in \Sigma_{g_N} \times U \times W \times Q$ such that*

$$
\begin{aligned}
a(\sigma; \tau) + b(u, \gamma, p; \tau) &= G(\tau) \quad \forall \, \tau \in \Sigma_0, \\
b(\sigma; v, \theta, q) + c(p; q) &= F(v) \quad \forall \, (v, \theta, q) \in U \times W \times Q.
\end{aligned}
\tag{1}
$$

Therein, Σ_{g_N} (respectively, Σ_0) denotes the Sobolev space $\Sigma = H(\mathrm{div}\,; \Omega)$ accounting for nonvanishing (respectively, vanishing) traction boundary conditions on Γ_N, while U, W and Q are Lebesgue spaces over the bounded domain $\Omega \subset \mathbb{R}^d$ with Lipschitz boundary $\Gamma = \Gamma_D \cup \Gamma_N$ for Dirichlet and traction boundary conditions. The bilinear forms $a(\cdot, \cdot)$, $b(\cdot, \cdot)$, and $c(\cdot, \cdot)$ are defined by

$$
a(\sigma; \tau) = \frac{1}{2\mu} \int_\Omega \sigma : \tau \, dx \qquad \forall \sigma, \tau \in \Sigma,
$$

$$
b(v, \theta, q; \tau) = \int_\Omega v \cdot \mathrm{div}\, \tau \, dx + \int_\Omega \theta \, \mathrm{As}\, \tau \, dx + \int_\Omega \frac{\varrho}{2} q \, \mathrm{Tr}\, \tau \, dx \\
\forall (v, \theta, q) \in U \times W \times Q \quad \forall \tau \in \Sigma_0,
$$

$$
c(p; q) = \int_\Omega \varrho \, p \, q \, dx \qquad \forall p, q \in Q,
$$

$$
\tag{2}
$$

where we set $\sigma : \tau = \sum_{i,j=1}^d \sigma_{ij} \tau_{ij}$, $\mathrm{Tr}\, \tau = \sum_{i=1}^d \tau_{ii}$ and, for $d = 2$, $\mathrm{As}\, \tau = \tau_{12} - \tau_{21}$. The linear forms $G(\tau)$ and $F(v)$ are defined by

$$
G(\tau) = \int_{\Gamma_D} u_D \cdot \tau \, n \, ds \quad \text{and} \quad F(v) = -\int_\Omega f \cdot v \, dx \quad \forall \tau \in \Sigma \; \forall v \in U.
$$

The parameter ϱ is a continuous function (also in the incompressible limit) of the compressibility modulus λ of the material. We refer the reader to Section 2 for the remaining details of notation.

Quasi-optimal and robust a priori error estimates for DMH were proved in [15]. Robustness here is referred to the performance of the DMH method in the sense that, for small values of the mesh size, the error is independent of the compressibility parameter. As anticipated before, the quasi-optimal convergence rate of DMH can be degraded by the presence of singularities in the computational domain, this demanding to resort to a robust mesh-refinining algorithm for an efficient automatic mesh-design. With this aim, we introduce in this paper explicit residual-based a posteriori error estimates for the DMH formulation. These a posteriori error estimates are used in an adaptive algorithm for effective automatic mesh generation (cf. Section 5).

For $d = 2$ and $\widetilde{\mathbb{C}} = 2\mu$, where μ is the second elastic Lamé coefficient, we propose the following error estimator with volume contribution η_K and edge contribution η_E: Given the computed discrete approximation $(\sigma_h, u_h, p_h, \gamma_h)$, we compute on each element K in the triangulation $\mathcal{T}_h$ the volume part of the refinement indicator

$$\eta_K^2 = \frac{h_K^2}{\mu^2}\|f + \mathrm{div}\,\sigma_h\|_{0,K}^2 + h_K^2\|\mathrm{curl}(\widetilde{\mathbb{C}}^{-1}\sigma_h + \frac{\varrho}{2}p_h\delta + \gamma_h)\|_{0,K}^2$$
$$+ \frac{1}{\mu^2}\|\mathrm{As}\,\sigma_h\|_{0,K}^2 + \|\frac{\varrho}{2}(p_h + \frac{1}{2}\mathrm{Tr}\,\sigma_h)\|_{0,K}^2.$$

Here and throughout the paper, $\|\cdot\|_{0,S}$ denotes the $L^2 = H^0$ norm $\|\cdot\|_{L^2(S)}$ on a domain, face or edge S. On each edge $E \in \mathcal{E}_h = \mathcal{E}_\Omega \cup \mathcal{E}_D \cup \mathcal{E}_N$, where $\mathcal{E}_\Omega$ denotes the set of interior edges, $\mathcal{E}_D$ and $\mathcal{E}_N$ the sets of edges on the Dirichlet and Neumann boundary, respectively, we compute the jump contribution to the refinement indicator

$$\eta_E^2 = \begin{cases} h_E\|J((\widetilde{\mathbb{C}}^{-1}\sigma_h + \frac{\varrho}{2}p_h\delta + \gamma_h)t_E)\|_{0,E}^2 & \text{if } E \in \mathcal{E}_\Omega, \\ h_E\|(\mathbb{C}^{-1}\sigma_h + \varrho/2\,p_h\delta + \gamma_h - \nabla u_D)t_E\|_{0,E}^2 & \text{if } E \in \mathcal{E}_D, \\ \dfrac{h_E}{\mu^2}\|\sigma_h\,n_E - g_N\|_{0,E}^2 & \text{if } E \in \mathcal{E}_N. \end{cases}$$

The error estimator associated with the DMH formulation, then reads

$$\Phi^2(\sigma_h; \mathcal{T}_h) := \sum_{K \in \mathcal{T}_h} \Phi_K^2 \quad \text{with} \quad \Phi_K^2 := \eta_K^2 + \sum_{E \in \partial K} \eta_E^2. \qquad (3)$$

Denoting by C_{rel} a positive constant independent of the mesh-size h and the material parameter $\lambda \in [0, \infty]$, the reliability of the error estimator is expressed by the following inequality

$$C_{\mathrm{rel}}^{-2} \|\widetilde{\mathbb{C}}^{-1/2}(\sigma - \sigma_h)\|_{0,\Omega}^2 \leq \varPhi^2(\sigma_h; \mathcal{T}_h). \qquad (4)$$

Details on the aformentioned notation are given in Sect. 2 and 3. The proof of (4) combines a unified approach from [9] with several arguments from [10, 11, 13, 12, 6]. Efficiency holds in a local form up to higher-order terms.

The local refinement indicator $\varPhi_K$ from (3) serves in an adaptive algorithm for effective automatic mesh generation. Numerical evidence in Section 6 supports that the resulting DMH adaptive scheme is characterized by optimal convergence rates when applied to the numerical solution of Lamé and Stokes benchmark problems with singularities.

The remaining part of the paper is organized as follows. Section 2 is devoted to the strong form of the linear elasticity problem and its related dual-mixed weak formulation. The numerical approximation of the DMH problem is then considered, and a priori quasi-optimal error estimates are reviewed for the method, with emphasis on their robustness with respect to the compressibility parameter. Section 2 concludes with some details on the efficient implementation of the dual-mixed method through the hybridization procedure; cf. [1, 2, 15]. A proof of the a posteriori error estimate (4) is given in Section 3 while efficiency of $\varPhi(\sigma_h; \tau_h)$ is discussed in Section 4. Section 5 illustrates the adaptive algorithm implemented in the computer code to drive the automatic mesh generation process. Numerical experiments on several benchmark problems illustrate in Section 6 the reliability and the efficiency of our robust a posteriori error estimate as well as the performance of the proposed adative refinement strategy.

2 Model problem, dual-mixed (hybrid) formulation, and finite element approximation

2.1 Mathematical model

Let $\Omega \subset \mathbb{R}^d$ be the reference configuration of an elastic material with Lipschitz boundary $\partial\Omega = \Gamma_D \cup \Gamma_N$, $\Gamma_D \neq \emptyset$, $\Gamma_D \cap \Gamma_N = \emptyset$, and its outward unit normal vector n. The linear elasticity problem reads: Given a volume force $f : \Omega \to \mathbb{R}^d$, a displacement $u_D : \Gamma_D \to \mathbb{R}^d$, a traction $g_N : \Gamma_N \to \mathbb{R}^d$, find a displacement $u : \Omega \to \mathbb{R}^d$ and a stress

$\sigma : \Omega \to M_{sym}^{d \times d} = \{\tau \in \mathbb{R}^{d \times d} : \tau = \tau^T\}$ satisfying

$$
\begin{aligned}
-\operatorname{div} \sigma &= f & &\text{in } \Omega, \\
\sigma &= \mathbb{C}\varepsilon(u) & &\text{in } \Omega, \\
u &= u_D & &\text{on } \Gamma_D, \\
\sigma\,n &= g_N & &\text{on } \Gamma_N
\end{aligned}
\tag{5}
$$

with strain tensor $\varepsilon(v) = \frac{1}{2}(\nabla v + (\nabla v)^T)$ and stress tensor

$$
\sigma = \mathbb{C}\epsilon(u) = 2\mu\epsilon(u) + \lambda \operatorname{Tr}\epsilon(u)\delta
\tag{6}
$$

in the isotropic case. In (6), λ, μ are the Lamé constants and δ is the $d \times d$ identity matrix. Plain strain or plane stress conditions can be recovered by taking in (5) appropriate values of the coefficients λ and μ (see [21], p.83).

Korn's inequality and Lax-Milgram lemma ensure that problem (5) admits a unique (weak) solution $(\sigma, u) \in L^2(\Omega; M_{sym}^{d \times d}) \times H^1(\Omega)^d$. In order to construct the DMH variational formulation of (5) we introduce two additional unknowns, p and γ, through the relations

$$
p = -\frac{1}{d} \operatorname{Tr}\sigma \quad \text{and} \quad \varepsilon(u) = \nabla u - \gamma.
\tag{7}
$$

The variable p is a *pressure parameter* that allows for a straightforward discrete treatment of the incompressible case ($\lambda = +\infty$) and is the main novelty of the DMH formulation with respect to the original PEERS approach [2]. Denoting by $\overline{p}$ the hydrostatic pressure, in the case $d = 3$ we have that $p = \overline{p}$, while when $d = 2$, $p = ((\lambda + \mu)/(\lambda + 2\mu/3))\overline{p}$ in the case of plain strain conditions and $p = 3\overline{p}/2$ in the case of plane stress conditions. The variable γ is the infinitesimal rotation tensor that allows to weaken the symmetry constraint on σ.

Introducing (7) into (5), we obtain the following equivalent formulation of the linear elasticity problem [15]: Find $u : \Omega \to \mathbb{R}^d$, $\sigma : \Omega \to M^{d \times d}$, $p : \Omega \to \mathbb{R}$, and $\gamma : \Omega \to M_{skew}^{d \times d} = \{\eta \in M^{d \times d} : \eta + \eta^T = 0\}$ such that

$$
\begin{aligned}
-\operatorname{div}\sigma &= f & &\text{in } \Omega, \\
\sigma &= \widetilde{\mathbb{C}}(\nabla u - \gamma) - \mu\varrho\,p\,\delta & &\text{in } \Omega, \\
p &= -\frac{1}{d}\operatorname{Tr}\sigma & &\text{in } \Omega, \\
\operatorname{As}\sigma &= 0 & &\text{in } \Omega, \\
u &= u_D & &\text{on } \Gamma_D, \\
\sigma\,n &= g_N & &\text{on } \Gamma_N
\end{aligned}
\tag{8}
$$

where $\widetilde{\mathbb{C}} = 2\mu$ and $\varrho = \lambda/(\mu(\lambda + 2\mu/d))$, with $\lim\limits_{\lambda \to \infty} \varrho = 1/\mu$. In the incompressible case, system (8) can be conveniently interpreted as the con-

servative form of the Stokes equations in fluid dynamics

$$
\begin{aligned}
-\mathrm{div}\,\sigma(u) &= f && \text{in } \Omega, \\
\sigma &= 2\nu\epsilon(u) - p\delta && \text{in } \Omega, \\
\mathrm{div}\,u &= 0 && \text{in } \Omega, \\
u &= u_D && \text{on } \Gamma_D, \\
\sigma(u)\,n &= g_N && \text{on } \Gamma_N
\end{aligned}
\tag{9}
$$

with kinematic viscosity $\nu = \mu$ and where u is to be intended as a velocity field. To show the equivalence of system (9) with the Stokes problem in conservative form, we use the definition of γ in $(8)_2$, take the trace of this latter relation, and use the definition of $\widetilde{\mathbb{C}}$ and p, obtaining

$$
\mathrm{Tr}\,\epsilon(u) = \mathrm{div}\,u = \frac{1}{2\mu}(\mathrm{Tr}\,\sigma + \mu\varrho\,pd) = \frac{p\,d}{2\mu}(\mu\varrho - 1).
$$

For $\lambda = +\infty$, the incompressibility constraint $\mathrm{div}\,u = 0$ is thus recovered.

2.2 DMH weak formulation

In order to introduce the DMH weak formulation of problem (8), we define the Sobolev space

$$
H(\mathrm{div}\,;\Omega) = \{\sigma \in L^2(\Omega; M^{d\times d}) :\ \mathrm{div}\,\sigma \in L^2(\Omega)^d\};
$$

and, given $u_D \in L^2(\Gamma_D)^d$, $g_N \in L^2(\Gamma_N)^d$ and $f \in L^2(\Omega)^d$,

$$
\begin{aligned}
\Sigma_{g_N} &= \{\sigma \in H(\mathrm{div}\,;\Omega) :\ \sigma n = g_N \text{ on } \Gamma_N\}, \\
U &= L^2(\Omega)^d, \quad W = L^2(\Omega; M^{d\times d}_{skew}), \quad Q = L^2(\Omega).
\end{aligned}
$$

In the case $\Gamma_N = \emptyset$, in order to preserve the uniqueness of the solution, the definition of the pressure space Q must be modified into $Q = L^2_0(\Omega)$, the space of square integrable functions over Ω having null average on Ω. Multiplying each equation in (8) by a proper test function and using integration by parts, we obtain the DMH weak formulation (1) of the linear elasticity problem. Under proper regularity assumptions on the solution of (8), an existence and uniqueness result of the solution of (1) has been proved in [15].

2.3 Finite element approximation

In view of the numerical approximation of problem (1) we assume henceforth that Ω is a bounded domain in $\mathbb{R}^2$ and we introduce a regular partition $\mathcal{T}_h$ [16] of Ω into triangles K such that $\overline{\Omega} = \bigcup_{K\in\mathcal{T}_h} \overline{K}$ and let $\mathcal{E}_h = \mathcal{E}_\Omega \cup \mathcal{E}_D \cup \mathcal{E}_N$ be the set of edges associated with $\mathcal{T}_h$. For each

element $K \in \mathcal{T}_h$ with boundary ∂K, we denote by $|K|$ and h_K the area and the diameter of K, respectively, while for each edge $E \in \mathcal{E}_h$ we denote by h_E the length of E and choose one unit normal n_E along E (pointing outwards Ω for $E \in \mathcal{E}_N$). We set $h = \max_{K \in \mathcal{T}_h} h_K$. Then, for $k \geq 0$, we denote by $\mathbb{P}_k(K)$ the space of polynomials in two variables of total degree at most k on the element K and we let $\mathbb{D}(K) = (\mathbb{RT}_0(K) \oplus \mathcal{B}_K)^2$, where $\mathbb{RT}_0(K)$ is the lowest order Raviart-Thomas finite element space [22] on K and $\mathcal{B}_K = \mathrm{curl}(b_K)$, b_K being the cubic bubble function on K [8]. The finite element spaces for the DMH approximation are defined as follows

$$
\begin{aligned}
\Sigma_{g_N,h} &= \{\sigma_h \in H(\mathrm{div}\,;\Omega) : \forall E \in \mathcal{E}_N, \, \sigma_h n|_E = \mathcal{P}_{0,E}(g_N); \\
&\qquad \forall K \in \mathcal{T}_h, \, \sigma_h|_K \in \mathbb{D}(K)\}, \\
U_h &= \{u_h \in U : \forall K \in \mathcal{T}_h, \, u_h|_K \in (\mathbb{P}_0(K))^2\}, \\
W_h &= \{\gamma_h \in C^0(\overline{\Omega}; M_{skew}^{2\times 2}) : \forall K \in \mathcal{T}_h, \, \gamma_h|_K \in \mathbb{P}_1(K; M_{skew}^{2\times 2})\}, \\
Q_h &= \{q_h \in Q : \forall K \in \mathcal{T}_h, \, q_h|_K \in \mathbb{P}_0(K)\}.
\end{aligned}
\tag{10}
$$

Therein, for any $E \in \mathcal{E}_h$, $\mathcal{P}_{0,E}$ is the orthogonal projection in $L^2(E)$ onto the space of constants $(\mathbb{P}_0(E))^2$ on E, i.e. $\mathcal{P}_{0,E}$ is the integral norm operator.

The discretization of problem (1) reads: *Find* $(\sigma_h, u_h, \gamma_h, p_h) \in \Sigma_{g_N,h} \times U_h \times W_h \times Q_h$ *such that*

$$
a(\sigma_h; \tau_h) + b(u_h, \gamma_h, p_h; \tau_h) = G(\tau_h) \quad \forall \, \tau_h \in \Sigma_{0,h},
$$

$$
b(\sigma_h; v_h, \theta_h, q_h) + c(p_h; q_h) = F(v_h) \quad \forall \, (v_h, \theta_h, q_h) \in U_h \times W_h \times Q_h.
\tag{11}
$$

Existence and uniqueness of the solution of the discretized problem (11) have been proved in [15] and in the same reference, under appropriate (minimal) regularity assumptions on the solution of problem (1), the following quasi-optimal a priori error estimates have been established

$$
\begin{aligned}
\|\sigma - \sigma_h\|_{0,\Omega} + \|p - p_h\|_{0,\Omega} &\lesssim h(|\sigma|_{1,\Omega} + |p|_{1,\Omega} + |\gamma|_{1,\Omega}), \\
\|u - u_h\|_{0,\Omega} &\lesssim h(|\sigma|_{1,\Omega} + |p|_{1,\Omega} + |u|_{1,\Omega} + |\gamma|_{1,\Omega}), \\
\|\gamma - \gamma_h\|_{0,\Omega} &\lesssim h(|\sigma|_{1,\Omega} + |p|_{1,\Omega} + |\gamma|_{1,\Omega}).
\end{aligned}
\tag{12}
$$

Here and throughout this paper, $A \leq CB$ is abbreviated as $A \lesssim B$ when C is a positive (generic) constant independent of h and independent of the compressibility parameter λ; for any integer $m \geq 0$ we denote by $\|\cdot\|_{m,S}$ and $|\cdot|_{m,S}$ the norm and seminorm on the Sobolev space $H^m(S)$, respectively, $S \subset \mathbb{R}^d$. It is important to notice that the above estimates are uniformly robust with respect to the compressibility parameter λ, i.e. they maintain their validity even in the exactly incompressible regime characterized by the value $\lambda = +\infty$.

The computer implementation of (11) leads to solving a linear sparse system of algebraic equations of large size. In order to reduce the computational complexity of the problem, it is convenient to resort to the hybridization of the dual-mixed formulation (11). This amounts to relaxing the $H(\mathrm{div}\,;\varOmega)$-continuity requirement for interelement normal stresses that is contained in the definition of the finite element space $\varSigma_{g_N,h}$ at the expense of introducing a further variable λ_h into the system (11) (see [1,2]). The variable λ_h is defined only over the edges of $\mathcal{E}_h$, this fact giving the name "hybrid" to the corresponding numerical scheme, and plays the role of a Lagrangian multiplier that enforces back the interelement traction reciprocity of the discrete stress σ_h. The resulting discontinuous finite element spaces for σ_h and λ_h are defined as

$$\varSigma_h = \{\sigma_h \in L^2(\varOmega; M^{2\times 2}) : \forall K \in \mathcal{T}_h,\, \sigma_h|_K \in \mathbb{D}(K)\},$$

$$\varLambda_{u_D,h} = \{\lambda_h \in L^2(\mathcal{E}_h)^2 : \forall E \in \mathcal{E}_h,\, \lambda_h|_E \in (\mathbb{P}_0(E))^2, \tag{13}$$

$$\forall E \in \mathcal{E}_D,\, \lambda_h|_E = \mathcal{P}_{0,E} u_D\}.$$

Since the stress σ_h is now a priori fully discontinuous over the triangulation $\mathcal{T}_h$, it can be statically eliminated at the element level together with the element displacement u_h, leading to a condensed system in the sole unknowns γ_h, p_h, λ_h (see [11,14] for the algorithmic details of the procedure). The interelement variable λ_h has the physical meaning of edge displacement and can be shown to enjoy a higher convergence rate than the corresponding element variable u_h (see [15] and also [1,18]).

3 A posteriori error estimate

This section is devoted to prove the reliability estimate (4). Beforehand, we need to introduce some notation that will be useful in the following.

3.1 Notation

For each edge $E \in \mathcal{E}_h$ with fixed normal n_E (that coincides with the exterior normal to $\varGamma$ if $E \subset \varGamma$), define the jump of a function v (that is continuous on each of the neighbouring elements K_+ and K_- but, in general, discontinuous along their intersection E) across the edge E as

$$J(v)|_E := (v|_{K_+}|_E) - (v|_{K_-}|_E),$$

K^+ being the triangle whose outward unit normal vector coincides with n_E. If $E = K \cap \varGamma$, we set

$$J(v)|_E := (v|_K|_E).$$

For each normal n_E we denote by t_E its associated tangent unit vector, such that n_E points to the right side defined by the orientation of t_E.

Moreover, we define

$$\text{Curl}\,\phi = (\phi_{,2} - \phi_{,1}), \qquad \text{curl}\,\phi = \begin{pmatrix} \phi_{,2} \\ -\phi_{,1} \end{pmatrix} \qquad \forall \phi \in H^1(\Omega);$$

$$\text{Curl}\,u = \begin{pmatrix} u_{1,2} & -u_{1,1} \\ u_{2,2} & -u_{2,1} \end{pmatrix}, \qquad \text{curl}\,u = u_{2,1} - u_{1,2} \qquad \forall u \in H^1(\Omega)^2;$$

$$\text{curl}\,\sigma = \begin{pmatrix} \sigma_{12,1} - \sigma_{11,2} \\ \sigma_{22,1} - \sigma_{21,2} \end{pmatrix}, \qquad \text{div}\,\sigma = \begin{pmatrix} \sigma_{11,1} + \sigma_{12,2} \\ \sigma_{21,1} + \sigma_{22,2} \end{pmatrix} \quad \forall \sigma \in H^1(\Omega; M^{2\times2}).$$

In the sequel, the mesh-size is regarded as a (piecewise constant) L^∞ function, i.e. $h_{\mathcal{T}_h}$ (respectively, $h_{\mathcal{E}_h}$) is $\mathcal{T}_h$-piecewise constant (respectively, $\mathcal{E}_h$-piecewise constant) with $h_{\mathcal{T}_h}|_K = h_K = \text{diam}(K)$ for each $K \in \mathcal{T}_h$ (respectively $h_{\mathcal{E}_h}|_E = h_E = \text{diam}(E)$ for each $E \in \mathcal{E}_h$). Similarly, the piecewise action of differential operators on (in general discontinuous) piecewise sufficiently smooth functions is denoted by a subindex, e.g. $\text{Curl}_{\mathcal{T}_h}$ means

$$(\text{Curl}_{\mathcal{T}_h} v)|_K = \text{Curl}(v|_K) \quad \text{for } v \in H^1(K), \quad \forall K \in \mathcal{T}_h.$$

For brevity, let $(\cdot, \cdot)_{0,S}$ denote the L^2 scalar product in $L^2(S)$ for a domain, edge etc. and let $\|\cdot\|_{0,S}$ denote the induced norm. Similarly, $\|\cdot\|_{1,S}$ and $|\cdot|_{1,S}$ denote the norm and seminorm in $H^1(S)$, respectively. Set $H^1_D(\Omega) := \{v \in H^1(\Omega)^d : v = 0 \text{ on } \Gamma_D\}$ and $H^1_0(\Omega) := \{v \in H^1(\Omega)^d : v = 0 \text{ on } \Gamma\}$ and

$$L := \{\sigma \in L^2(\Omega; M^{d\times d}_{\text{sym}}) : \int_\Omega \text{Tr}\,(\sigma)\,dx = 0\} \text{ and } V := H^1_0(\Omega)^d \text{ if } \Gamma_N = \emptyset;$$

$$L := L^2(\Omega; M^{d\times d}_{\text{sym}}) \text{ and } V := H^1_D(\Omega) \text{ if } \Gamma_N \neq \emptyset.$$

Let $\|\cdot\|_L := \|\cdot\|_{0,\Omega}$ and $\|\cdot\|_V := \|\cdot\|_{1,\Omega}$. With the elasticity tensor $\mathbb{C}$ from (6) and the positive parameters μ and λ one defines the energy norms

$$\|\varepsilon(v)\|_{\mathbb{C}} := (\mathbb{C}\varepsilon(v), \varepsilon(v))^{1/2}_{0,\Omega} \quad \text{and} \quad \|\tau\|_{\mathbb{C}^{-1}} := (\mathbb{C}^{-1}\tau, \tau)^{1/2}_{0,\Omega}$$

for any $\varepsilon(v)$ or τ in $L^2(\Omega; M^{2\times2})$.

3.2 Mathematical preliminaries

Given the exact and discrete solution (σ, u, γ, p) and $(\sigma_h, u_h, \gamma_h, p_h)$ in $H(\text{div}; \Omega) \times U \times W \times Q$, define $\tilde{\sigma}_h := \text{sym}\,\sigma_h$, the symmetric part of σ_h and let $w \in H^1(\Omega)^2$ be some Sobolev function with $w = u_D$ on Γ_D.

Since, $\tilde{\sigma}_h$ does, in general, not equal $\mathbb{C}\varepsilon(\tilde{u}_h)$ for some $\tilde{u}_h \in H_D^1(\Omega)$, we consider that $\tilde{u}_h + w \in H_D^1(\Omega)$ with the minimal distance with respect to $\mathbb{C}\varepsilon(\tilde{u}_h)$ as defined by the following Helmholtz decomposition.

Lemma 1 (Helmholtz decomposition for symmetric tensor fields, [10])
Suppose that Γ_N is a finite union of connected components $\Gamma_0, \ldots, \Gamma_M$ and either $\Gamma_N = \emptyset$ or $\Gamma_N \neq \emptyset$ and Γ_D have a positive distance. Then there exists $\tilde{u}_h \in H_D^1(\Omega)$ and $\Phi \in H^2(\Omega)$ with $\int_\Omega \Phi \, dx = 0$, $\mathrm{Curl}\,\Phi = c_j$ on Γ_j, $c_j \in \mathbb{R}^2$, $j = 1, \ldots, M$, $c_0 = 0$, such that

$$\tilde{\sigma}_h - \mathbb{C}\varepsilon(w) = \mathbb{C}\varepsilon(\tilde{u}_h) + \mathrm{Curl}\,\mathrm{Curl}\,\Phi. \qquad \square \qquad (14)$$

Lemma 2 ([10]) *There exists some λ-independent constant C_1 (which depends on Γ_N, Ω, and μ but not on λ or on Φ) such that*

$$\|\Phi\|_{2,\Omega} = \|\mathrm{Curl}\,\mathrm{Curl}\,\Phi\|_{0,\Omega} \leq C_1 \|\mathrm{Curl}\,\mathrm{Curl}\,\Phi\|_{\mathbb{C}^{-1}}. \square$$

Theorem 3 *Let $\mathcal{A} : L \times V \to (L \times V)'$ be defined by*

$$(\mathcal{A}(\sigma, u))(\tau, v) := (\mathbb{C}^{-1}\sigma, \tau)_{0,\Omega} - (\sigma, \varepsilon(v))_{0,\Omega} - (\tau, \varepsilon(u))_{0,\Omega}$$

for all $\sigma, \tau \in L$ and $u, v \in V$. Then, the operator $\mathcal{A}$ is bounded and bijective and the operator norms of $\mathcal{A}$ and $\mathcal{A}^{-1}$ are λ-independent.

Proof. The case $\Gamma_N = \emptyset$ is proved in [6, Theorem 5.1] and the proof in the case $\Gamma_N \neq \emptyset$ is sketched in the sequel for convenient reading. We refer the reader to [5,8] for the general theory of mixed formulations. The continuity and inf-sup condition on the bilinear form $(\sigma, \varepsilon(u))$ (with λ-independent constants) are well established. The kernel of this bilinear form reads

$$Z := \{\sigma \in L : \, \mathrm{div}\,\sigma = 0 \text{ in } \Omega \text{ and } \sigma n = 0 \text{ on } \Gamma_N\}.$$

The remaining non-trivial point is to verify that the bilinear form $(\mathbb{C}^{-1}\sigma, \tau)$ is continuous and Z-elliptic with λ-independent constants. The first property is immediate from the expression of $\mathbb{C}^{-1}$. To check the latter property, given $\sigma \in Z$, we employ the arguments of Lemma 1 and obtain

$$\sigma = \mathbb{C}\varepsilon(v) + \mathrm{Curl}\,\mathrm{Curl}\,\Phi$$

for $v \in H_D^1(\Omega)$ and Φ with properties stated in the lemma. Since $\mathrm{div}\,\sigma = 0$ in Ω and $\sigma n = 0 = \mathrm{Curl}\,\mathrm{Curl}\,\Phi n$ on Γ_N we deduce $v = 0$. From Lemma 4.2 in [10] we have

$$\|\mathrm{Curl}\,\mathrm{Curl}\,\Phi\|_{0,\Omega} \leq C_1 \|\mathrm{Curl}\,\mathrm{Curl}\,\Phi\|_{\mathbb{C}^{-1}}$$

for a λ-independent constant C_1 (which depends on Γ_N, Ω, and μ but not on Φ). Since $\sigma = \mathrm{Curl}\,\mathrm{Curl}\,\Phi$, the last inequality reads $C_1^{-2}\|\sigma\|_L^2 \leq (\mathbb{C}^{-1}\sigma, \sigma)$. For more details cf. [6]. $\square$

3.3 Proof of reliability.

Recall that $w \in H^1(\Omega)^d$ denotes a function with $w = u_D$ on Γ_D and recall from (14), that

$$\sigma - \tilde{\sigma}_h = \mathbb{C}\varepsilon(u - w - \tilde{u}_h) - \operatorname{Curl}\operatorname{Curl}\Phi.$$

Theorem 3 is then applied to $(\sigma - \tilde{\sigma}_h, u - w - \tilde{u}_h)$ and yields existence of $(\tau, v) \in L \times V$ with $\|(\tau, v)\|_{L \times V} \lesssim 1$ uniformly bounded such that

$$
\begin{aligned}
\|\sigma &- \tilde{\sigma}_h\|_L + \|u - w - \tilde{u}_h\|_V \\
&= (\mathcal{A}(\sigma - \tilde{\sigma}_h, u - w - \tilde{u}_h))(\tau, v) \\
&= (\mathbb{C}^{-1}(\sigma - \tilde{\sigma}_h), \tau)_{0,\Omega} - (\sigma - \tilde{\sigma}_h, \varepsilon(v))_{0,\Omega} \\
&\quad - (\tau, \varepsilon(u - w - \tilde{u}_h))_{0,\Omega} \\
&= -(\operatorname{Curl}\operatorname{Curl}\Phi, \tau)_{0,\Omega} - (\sigma, \varepsilon(v))_{0,\Omega} + (\sigma_h, \varepsilon(v))_{0,\Omega}
\end{aligned}
\tag{15}
$$

because of $\mathbb{C}^{-1}\sigma = \varepsilon(u)$ and $\tilde{\sigma}_h : \varepsilon(v) = \sigma_h : \varepsilon(v)$.

In the next steps, we estimate the right-hand side of (15).

Using $(\sigma, \varepsilon(v))_{0,\Omega} = (f, v)_{0,\Omega} + \int_{\Gamma_N} g_N\, v\, ds$ and an integration by parts in the term $(\sigma_h, \nabla v)_{0,\Omega}$ we obtain

$$
\begin{aligned}
\|\sigma - \tilde{\sigma}_h\|_L + \|u - w - \tilde{u}_h\|_V = (-\operatorname{Curl}\operatorname{Curl}\Phi, \tau)_{0,\Omega} - (\operatorname{div}\sigma_h + f, v)_{0,\Omega} \\
+ (\sigma_h, \varepsilon(v) - \nabla v)_{0,\Omega} + \int_{\Gamma_N} (\sigma_h\, n - g_N) v\, ds.
\end{aligned}
$$

Since $\int_K (f + \operatorname{div}\sigma_h)\, dx = 0$ for any $K \in \mathcal{T}_h$ we have, with $v_h \in (\mathbb{P}_0(\mathcal{T}_h))^2$ defined by $v_h|_K := |K|^{-1} \int_K v(x)\, dx$ for all $K \in \mathcal{T}_h$, that

$$
\begin{aligned}
-(\operatorname{div}\sigma_h + f, v)_{0,\Omega} &= -(\operatorname{div}\sigma_h + f, v - v_h)_{0,\Omega} \\
&\leq \|h_{\mathcal{T}_h}(f + \operatorname{div}\sigma_h)\|_{0,\Omega} \|h_{\mathcal{T}_h}^{-1}(v - v_h)\|_{0,\Omega} \\
&\lesssim \|h_{\mathcal{T}_h}(f + \operatorname{div}\sigma_h)\|_{0,\Omega}
\end{aligned}
$$

(owing to an elementwise Poincare inequality $\|h_{\mathcal{T}_h}^{-1}(v - v_h)\|_{0,\Omega} \leq 1/\pi\, \|\nabla v\|_{0,\Omega} \leq 1$). Since $\sigma_h\, n|_E = \mathcal{P}_{0,E} g_N$ for each $E \in \mathcal{E}_N$, a similar argument shows that

$$
\begin{aligned}
\int_{\Gamma_N} (\sigma_h\, n - g_N) v\, ds &= \int_{\Gamma_N} (\sigma_h\, n - g_N)(v - v_{\mathcal{E}_h})\, dx \\
&\leq \|h_{\mathcal{E}_h}^{1/2}(g_N - \sigma_h\, n)\|_{0,\Gamma_N} \|h_{\mathcal{E}_h}^{-1/2}(v - v_\varepsilon)\|_{0,\Gamma_N} \\
&\lesssim \|h_{\mathcal{E}_h}^{1/2}(g_N - \sigma_h\, n)\|_{0,\Gamma_N}
\end{aligned}
$$

(owing to an elementwise trace inequality and a proper choice of an edge-wise $v_{\mathcal{E}_h}$).

Since $(\sigma_h, \varepsilon(v) - \nabla v)_{0,\Omega} = (As \sigma_h, \varepsilon(v) - \nabla v)_{0,\Omega}$, this term is bounded by $\|As \sigma_h\|_{0,\Omega}^2 \|\varepsilon(v) - \nabla v\|_{0,\Omega}^2 \lesssim \|As \sigma_h\|_{0,\Omega}^2$ (where we employed Korn's inequality and $\|v\|_V \leq 1$ in the last step).

Altogether, we deduce

$$\|\sigma - \tilde{\sigma}_h\|_L + \|u - w - \tilde{u}_h\|_V \lesssim \|\operatorname{Curl}\operatorname{Curl}\Phi\|_L + \|h_{\mathcal{T}_h}(f + \operatorname{div}_{\mathcal{T}_h}\sigma_h)\|_{0,\Omega}$$
$$+ \|h_{\mathcal{E}_h}^{1/2}(g_N - \sigma_h n)\|_{0,\Gamma_N} + \|As \sigma_h\|_L. \quad (16)$$

Lemma 4 *There exists a (λ, h)-independent constant $C_2 > 0$ such that*

$$\|\operatorname{Curl}\operatorname{Curl}\Phi\|_{\mathbb{C}^{-1}} \leq C_2 \left(\|h_{\mathcal{T}_h}\operatorname{Curl}_{\mathcal{T}_h}(\tilde{\mathbb{C}}^{-1}\sigma_h + \varrho/2\, p_h\delta + \gamma_h)\|_{0,\Omega} \right.$$
$$\left. + \|h_{\mathcal{E}_h}^{1/2} J(\tilde{\mathbb{C}}^{-1}\sigma_h + \varrho/2\, p_h\delta + \gamma_h)t_E\|_{0,(\Gamma \cup \mathcal{E}_\Omega \cup \Gamma_D)} \right).$$

Proof. Notice that

$$\mathbb{C}^{-1}\tilde{\sigma}_h = \tilde{\sigma}_h/(2\mu) - \lambda/(2\mu)(\operatorname{Tr}\tilde{\sigma}_h)\delta/(2\lambda + 2\mu)$$
$$= \tilde{\mathbb{C}}^{-1}\tilde{\sigma}_h - \varrho/4\operatorname{Tr}(\sigma_h)\delta$$

and abbreviate

$$\hat{\sigma}_h := \tilde{\mathbb{C}}^{-1}\sigma_h + \varrho/2\, p_h\delta + \gamma_h.$$

The orthogonality in the Helmholtz decomposition (14) leads to

$$\|\operatorname{Curl}\operatorname{Curl}\Phi\|_{\mathbb{C}^{-1}}^2 = \int_\Omega \operatorname{Curl}\operatorname{Curl}\Phi : (\mathbb{C}^{-1}\tilde{\sigma}_h - \varepsilon(w))\, dx$$
$$= (\operatorname{Curl}\operatorname{Curl}\Phi, \hat{\sigma}_h)_{0,\Omega} - (\operatorname{Curl}\operatorname{Curl}\Phi, \varrho/2(p_h$$
$$+ 1/2\operatorname{Tr}(\sigma_h)))\delta)_{0,\Omega} - (\operatorname{Curl}\operatorname{Curl}\Phi, \nabla w)_{0,\Omega}$$

where we have already used the aforementioned notation and the fact that $\operatorname{Curl}\operatorname{Curl}\Phi$ is symmetric (and so orthogonal to asymmetric $\sigma_h - \tilde{\sigma}_h$ and γ_h). Lemma 2 yields

$$\|\operatorname{Curl}\operatorname{Curl}\Phi\|_L \lesssim (\operatorname{Curl}\operatorname{Curl}\Phi, \hat{\sigma}_h - \nabla w)_{0,\Omega} + \|\varrho/2(p_h + 1/2\operatorname{Tr}(\sigma_h))\|_{0,\Omega}.$$

The estimation of $(\operatorname{Curl}\operatorname{Curl}\Phi, \hat{\sigma}_h)_{0,\Omega}$ essentially follows the technique of [10, Lemma 5.1]. The first observation is that $b := \operatorname{Curl}\Phi \in H^1(\Omega)^2$ is constant on each of the connectivity components Γ_j of Γ_N. Taking nodal interpolation as a boundary condition on Γ_N and a Clement-type weak interpolant, e.g. $b_h(z) := |\omega_z|^{-1} \int_{\omega_z} b(x)\, dx$ for a node $z \notin \overline{\Gamma}_N$ with patch

$\omega_z := \text{int}(\cup\{K \in \mathcal{T}_h : z \in K\})$ and $b_h(z) := b(z) = c_j$ for $z \in \overline{\Gamma}_j$, one defines $b_h \in C(\overline{\Omega})^2 \cap (\mathbb{P}_1(\mathcal{T}_h))^2$ with $b - b_h = 0$ on Γ_N and so is $\text{Curl}\, bn = 0 = \text{Curl}\, bn$ almost everywhere Γ_N. Furthermore,

$$\|h_{\mathcal{T}_h}^{-1}(b - b_h)\|_{0,\Omega} + \|h_{\mathcal{E}_h}^{-1/2}(b - b_h)\|_{0,\mathcal{E}_h} \lesssim |b|_{1,\Omega} \lesssim |\Phi|_{2,\Omega}. \qquad (17)$$

Since $\text{Curl}\, b_h \in P_0(\mathcal{T}; \mathbb{M}^{2\times 2})$ with $\text{div}\,\text{Curl}\, b_h = 0$, $\tau_h := \text{Curl}\, b_h \in \Sigma_{0,h}$ and $(11)_1$ yield

$$\int_{\Gamma_D} u_D \cdot \tau_h\, n\, ds = (\tilde{\mathbb{C}}^{-1}\sigma_h, \tau_h)_{0,\Omega} + (\gamma_h, \text{As}\,\tau_h)_{0,\Omega}$$
$$+ (\varrho/2\, p_h, \text{Tr}\,\tau_h)_{0,\Omega} = (\widehat{\sigma}_h, \tau_h)_{0,\Omega}.$$

This and $\tau_h n = 0$ along Γ_N plus an integration by parts show that

$$(\hat{\sigma}_h, \tau_h)_{0,\Omega} = \int_{\Gamma_D} w_D \cdot \text{Curl}\, b_h n\, ds = \int_{\Gamma} w \cdot \text{Curl}\, b_h n\, ds = (\text{Curl}\, b_h, \nabla w)_{0,\Omega}.$$

Therefore,

$$(\text{Curl}\,\text{Curl}\,\Phi, \hat{\sigma}_h - \nabla w)_{0,\Omega} = (\text{Curl}(b - b_h), \hat{\sigma}_h - \nabla w)_{0,\Omega}.$$

A standard piecewise integration by parts yields

$$(\text{Curl}\,\text{Curl}\,\Phi, \hat{\sigma}_h - \nabla w)_{0,\Omega} = (b - b_h, \text{Curl}_{\mathcal{T}_h}\,\hat{\sigma}_h)_{0,\Omega}$$
$$- \int_{\cup\mathcal{E}_\Omega} (b - b_h) \cdot J(\hat{\sigma}_h) t_E\, ds$$
$$- \int_{\Gamma_D} (b - b_h)(\hat{\sigma}_h t_E - \partial u_D/\partial s)\, ds.$$

From this, using Cauchy inequalities, trace estimates and (17), we eventually conclude the proof; cf. [10] for further details. $\quad\square$

Lemma 4 and inequality (16) show that

$$\|\sigma - \tilde{\sigma}_h\|_L + \|u - w - \tilde{u}_h\|_V \lesssim \|h_{\mathcal{T}_h}\,\text{Curl}_{\mathcal{T}_h}(\tilde{\mathbb{C}}^{-1}\sigma_h + \varrho/2\, p_h\delta + \gamma_h)\|_{0,\Omega}$$
$$+ \|h_{\mathcal{E}_h}^{1/2} J(\tilde{\mathbb{C}}^{-1}\sigma_h + \varrho/2\, p_h\delta + \gamma_h) t_E\|_{0,\cup\mathcal{E}_h}$$
$$+ \|h_{\mathcal{T}_h}(f + \text{div}_{\mathcal{T}_h}\sigma_h)\|_{0,\Omega} + \|h_{\mathcal{E}_h}^{1/2}(g_N - \sigma_h n)\|_{0,\Gamma_N} + \|\text{As}\,\sigma_h\|_L.$$

This is the reliability of our proposed estimator in a slightly different notation.

4 Efficiency

Given the reliable error estimator with η_K and η_E, this section aims to establish the reverse estimate for η_K and η_E even in a local form: For each $K \in \mathcal{T}_h$, it can be proved that

$$\eta_K \lesssim \|\sigma - \sigma_h\|_{0,K} + \|p - p_h\|_{0,K} + \|\gamma - \gamma_h\|_{0,K} + h_K\|f - f_K\|_{0,K}.$$
(18)

The last term $\|h_K(f - f_K)\|_{0,K}$, with the integral mean f_K of f on K, is an oscillation of the right-hand side and is of higher order (provided $f \in H^1(K)$). The proof of (18) is by a standard inverse estimate technique due to Verfürth [23]. We therefore give an example for $\|h_K(\operatorname{Curl} \hat{\sigma}_h)\|_{0,K} =:$ $\varrho_1(\hat{\sigma}_h)$ and the polynomial $\hat{\sigma}_h := \tilde{\mathbb{C}}^{-1}\sigma_h + \varrho/2\,p_h\delta + \gamma_h$ on K of degree $\lesssim 2$, written $\hat{\sigma}_h \in \mathbb{P}(K)$.

On the finite-dimensional vector space $\mathbb{P}(K)$, ϱ_1 is a seminorm and so we have

$$\varrho_2(\hat{\tau}_h) := \min_{v \in H^1(\Omega)} \|\hat{\tau}_h - \nabla v\|_{0,K} \quad \text{for } \hat{\tau}_h \in \mathbb{P}(K).$$

Notice that $\varrho_2(\hat{\tau}_h) = 0$ implies that $\hat{\tau}_h$ is a gradient and hence $\varrho_1(\hat{\tau}_h) = 0$. Owing to the equivalence of norms on finite dimensional vector spaces (here, a quotient space of $\mathbb{P}(K)$ factorized by the set of gradients) one deduces that $\varrho_1 \lesssim \varrho_2$. A scaling argument reveals that the constant C in $\varrho_1 \leq C\varrho_2$ on $\mathbb{P}(K)$ is independent of h_K. Therefore, we have that

$$\|h_K \operatorname{Curl} \hat{\sigma}_h\|_{0,K} \lesssim \|\tilde{\mathbb{C}}^{-1}(\sigma - \sigma_h) + \varrho/2(p - p_h)\delta + \gamma - \gamma_h\|_{0,K}$$

and triangle inequalities yield the associated result in (18). The remaining assertions in (18) are easier to prove; we therefore omit further details on η_K.

The interior edge contributions η_E for $E \in \mathcal{E}_\Omega$ satisfy

$$h_E^{1/2}\|J((\tilde{C}^{-1}\sigma_h + \varrho/2\,p_h\delta + \gamma_h)t_E)\|_{0,E}$$
$$\lesssim \|\sigma - \sigma_h\|_{0,\omega_E} + \|p - p_h\|_{0,\omega_E} + \|\gamma - \gamma_h\|_{0,\omega_E} + \|h_\mathcal{T}(f - f_\mathcal{T})\|_{0,\omega_E}$$
(19)

with a right-hand side that is the sum of the right-hand side in (18) for the two neighbouring elements $K = T_\pm$, $\overline{\omega}_E = T_+ \cup T_-$ and $T_\pm \in \mathcal{T}_h$ with $T_+ \cap T_- = E$. The proof of (19) follows the lines of that of (18) on the finite dimensional space $\mathbb{P}(T_+) \oplus \mathbb{P}(T_-)$ of piecewise polynomial functions on ω_E (and $\|\hat{\tau}_h - \nabla v\|_{0,\omega_E}$) in the definition of ϱ_2. We therefore omit further details and, instead, mention the standard technique for the

proof of (18)-(19) which employs cubic and quadratic bubble-functions and an integration by parts. In this way, one can prove that η_E is efficient for $E \in \mathcal{E}_{D} \cup \mathcal{E}_N$ in the following sense

$$\eta_E \lesssim h_E^{1/2} \|\sigma_h n_E - g_N\|_{0,E}$$

$$\lesssim \|\sigma - \sigma_h\|_{0,\omega_E} + \|h_E(f - f_{\mathcal{T}_h})\|_{0,\omega_E} + h_E^{1/2}\|g_N - g_{N,E}\|_{0,E} \quad \forall E \in \mathcal{E}_N,$$

$$\eta_E \lesssim h_E^{1/2} \|(\tilde{\mathbb{C}}^{-1}\sigma_h + \varrho/2\, p_h\delta + \gamma_h - \nabla u_D)t_E\|_{0,E}$$

$$\lesssim h_E^{1/2}\|(\tilde{\mathbb{C}}^{-1} + \varrho/2\, p_h\delta + \gamma_h - \nabla u_{D,E})t_E\|_{0,E} + h_E^{1/2}\|\partial/\partial s\,(u_D - u_{D,E})\|_{0,E}$$

$$\lesssim \|\sigma - \sigma_h\|_{0,\omega_E} + \|p - p_h\|_{0,\omega_E} + \|\gamma - \gamma_h\|_{0,\omega_E} + h_E^{1/2}|u_D - u_{D,E}|_{1,E}$$

for all $E \in \mathcal{E}_D$. Therein, $\overline{\omega}_E = K \in \mathcal{T}_h$ is the neighbouring element of $E \subseteq K \cap \Gamma$ and, at least for smooth data g_N and u_D, $g_{N,E}$ and $u_{D,E}$ are their constant and affine approximations on E, respectively. Further details on the adopted arguments can be found in [10, 11] and are therefore omitted here.

5 Adaptive algorithm

The efficiency in the local form asserted above motivates the usage of Φ_K^2 as a refinement indicator in an adaptive mesh-refining algorithm.

The following adaptive Algorithm (A) has been implemented in the framework of a `Matlab` computer code:

a. Start with a coarse mesh $\mathcal{T}_{h,0}$, $k = 0$, and a fixed tolerance `tol` > 0.
b. Solve the discrete problem with respect to the present mesh $\mathcal{T}_{h,k}$ with N degrees of freedom.
c. Compute Φ_K for all $K \in \mathcal{T}_{h,k}$ with a sum over all the edges E of K.
d. Compute the error estimate

$$\Phi_k = \Phi_k(\sigma_h; \mathcal{T}_{h,k}) = \Big(\sum_{K \in \mathcal{T}_{h,k}} \Phi_K^2\Big)^{1/2}$$

corresponding to the mesh $\mathcal{T}_{h,k}$. Then, terminate the algorithm if

$$\Phi_k \leq \texttt{tol}\, \Phi_0,$$

otherwise go to step (e) of the algorithm.
e. Mark the element K for further refinement if $\Phi_K \geq \dfrac{1}{2} \max\limits_{K' \in \mathcal{T}_{h,k}} \Phi_{K'}$.

f. Perform red-green-blue refinement on all the marked elements and run a closure algorithm to avoid hanging nodes.
g. Generate the new mesh $\mathcal{T}_{h,k+1}$, set $k \to k + 1$, and go to (b).

Details on the *red-green-blue* refinement and closure algorithms can be

found in [24, 17, 7]. The numerical performance of Algorithm (A) will be illustrated in Section 6 in the solution of several compressible and incompressible benchmark problems with singularities.

6 Numerical experiments

To provide experimental evidence of the robustness and accuracy of the DMH method with adaptive mesh refinement and of the reliability, efficiency and robustness of the a-posteriori error estimator, we investigate several model problems, both in the incompressible (Stokes problem) and in the compressible regime. We also compare the results provided by algorithm (A) with uniform mesh-refinement. In the following, the parameter N represents the total number of degrees of freedom associated with a certain mesh, while h represents an average mesh size (in the case of uniform refinement).

6.1 Stokes flow in an L-shaped domain

The first numerical example deals with the solution of the Stokes problem in the L-shaped domain shown in Fig. 1, with $f = 0$ and viscosity $\mu = 1$. The boundary values, prescribed as specified in Fig. 1 (left), are computed from the exact solution, which reads as a function of the polar coordinates (r, θ)

$$u = r^\alpha((1 + \alpha)\sin(\theta)w(\theta) + \cos(\theta)w_\theta(\theta)),$$
$$v = r^\alpha(-(1 + \alpha)\cos(\theta)w(\theta) + \sin(\theta)w_\theta(\theta)), \qquad (20)$$
$$p = -r^{(\alpha-1)}((1 + \alpha)^2 w_\theta(\theta) + w_{\theta\theta\theta}(\theta))/(1 - \alpha),$$

with

$$w(\theta) = (\sin((1 + \alpha)\theta)\cos(\alpha\omega))/(1 + \alpha) - \cos((1 + \alpha)\theta)$$
$$-(\sin((1 - \alpha)\theta)\cos(\alpha\omega))/(1 - \alpha) + \cos((1 - \alpha)\theta),$$

and where $\alpha = 0.54448373$ is the positive solution of the equation $\alpha\sin(2\omega) + \sin(2\omega\alpha) = 0$, with $\omega = 3\pi/2$.

A plot of the initial mesh is given in Fig. 1 (right), while in Fig. 2 we show the mesh generated by Algorithm (A) after 12 refinement steps and a magnified detail of the mesh around the re-entrant corner at $(0, 0)$. Notice the strong nonuniformity of the computational mesh and the high refinement performed by the automatic mesh generation algorithm near the singularity.

The experimental convergence rate for the uniform refinement tends to the theoretically expected rate α which results from the approximation of
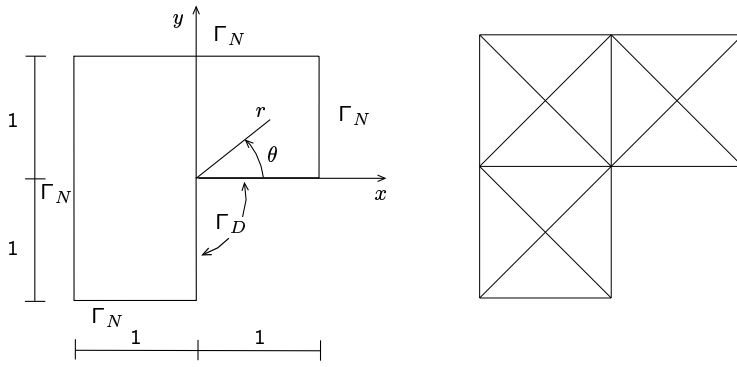
Figure 1. Computational domain (left) and initial mesh (right) for test case 6.1.
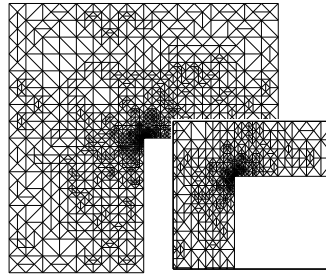

Figure 2. Adaptive mesh generated by Algorithm (A) after 12 refinement steps with a magnified detail around the re-entrant corner at $(0, 0)$ for test case 6.1.

singular functions like (20) (see [19]). The convergence rate we obtain with the adaptive mesh refinement is improved to the optimal order 1. These results are shown in Fig. 3, where the error $|||\sigma - \sigma_h||| = ||\widetilde{C}^{-1/2}(\sigma - \sigma_h)||_{0,\Omega}$ and the error estimator $\Phi(\sigma_h; \mathcal{T}_h)$ are displayed as functions of N on uniform and adaptive meshes (notice that in Fig. 3, a slope 1/2 corresponds to a convergence rate of 1).

In Tab. 1 we show the error $|||\sigma - \sigma_h|||$ and the error $||u - u_h||_{0,\Omega}$, both computed using a high-order Gauss quadrature formula on each mesh element.

The experimental convergence rate CR is defined as the corresponding (negative) slope in Fig. 3. We observe that the quotient $\frac{\Phi(\sigma_h; \mathcal{T}_h)}{|||\sigma - \sigma_h|||}$ remains bounded from above in agreement with estimate (4).
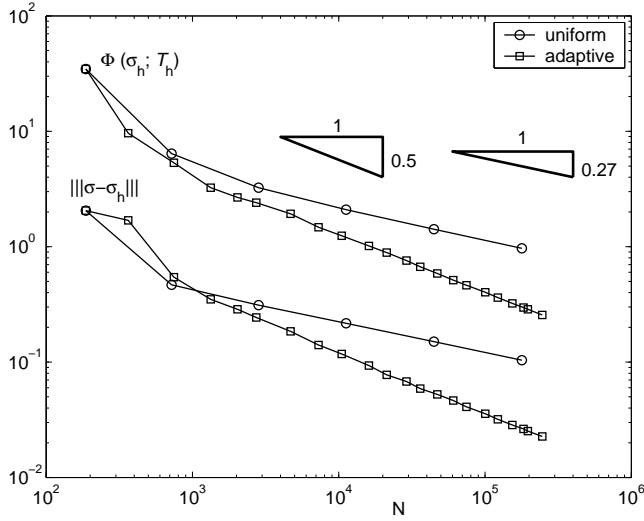
Figure 3. Error and error estimator for test case 6.1 on uniform and adaptive meshes.

N	h	$\|\|\|\sigma - \sigma_h\|\|\|$	CR	$\|\|u - u_h\|\|_{0,\Omega}$	CR	$\frac{\Phi(\sigma_h;\mathcal{T}_h)}{\|\|\|\sigma-\sigma_h\|\|\|}$
187	1.4142	2.052e+00	-	8.728e+00	-	0.0592
721	0.7071	4.673e-01	2.135	5.643e-01	3.951	0.0730
2833	0.3536	3.118e-01	0.584	1.940e-01	1.540	0.0961
11233	0.1770	2.169e-01	0.523	8.188e-02	1.244	0.1036
44737	0.0884	1.505e-01	0.527	3.716e-02	1.139	0.1063
178561	0.0442	1.038e-01	0.534	1.740e-02	1.094	0.1075

Table 1. Error and convergence rates on uniform meshes for test case 6.1.

In Tab. 1 we show the individual contributions to the error estimator, defined as follows

$$\eta_{\text{curl}} = \sum_{K \in \mathcal{T}_h} \left(\|\text{curl}(\widetilde{\mathbb{C}}^{-1}\sigma_h + \frac{\rho}{2}p_h\delta + \gamma_h)\|_{0,K}^2 \right)^{1/2},$$

$$\eta_{\text{As}} = \sum_{K \in \mathcal{T}_h} \left(\frac{1}{\mu^2}\|\text{As}\,\sigma_h\|_{0,K}^2 \right)^{1/2},$$

$$\eta_E = \sum_{e \in \mathcal{E}_\Omega \cup \mathcal{E}_D} \left(h_E\|J((\widetilde{\mathbb{C}}^{-1}\sigma_h + \frac{\rho}{2}p_h\delta + \gamma_h - \nabla u_D)t_E)\|_{0,E}^2 \right.$$
$$\left. + \sum_{e \in \mathcal{E}_N} \frac{h_E}{\mu^2}\|\sigma_h\,n_E - g_N\|_{0,E}^2 \right)^{1/2}.$$

The remaining contributions to the error estimator, $\eta_{div} = \sum_{K \in \mathcal{T}_h} \left(\frac{h_K^2}{\mu^2}\|f + \text{div}\,\sigma_h\|_{0,K}^2 h_K^2 \right)^{1/2}$ and $\eta_{Tr} = \sum_{K \in \mathcal{T}_h} \left(\|\frac{\rho}{2}(p_h + \frac{1}{2}\text{Tr}\,\sigma_h)\|_{0,K}^2 \right)^{1/2}$, here as

well as in the following examples, are of negligible size compared to the other contributions.

N	h	η_{curl}	CR	η_{As}	CR	η_E	CR
187	1.4142	1.939e+01	-	1.010e+01	-	2.685e+01	-
721	0.7071	3.405e+00	2.509	2.071e+00	2.286	5.001e+00	2.424
2833	0.3536	1.475e+00	1.207	1.167e+00	0.827	2.638e+00	0.922
11233	0.1770	9.156e-01	0.688	7.725e-01	0.595	1.716e+00	0.620
44737	0.0884	6.156e-01	0.572	5.238e-01	0.560	1.161e+00	0.563
178561	0.0442	4.195e-01	0.553	3.577e-01	0.550	7.935e-01	0.550

Table 2. Individual contributions to the error estimator on uniform meshes.

6.2 Stokes flow over a backward facing step

As a next example, we consider a fluid flow through a backward facing step as shown in Fig. 4, with $\mu = 1/50$. On Γ_N we set

$$g = (68, (2y - 3)/1100) \qquad x = 0, \ y \in [1, 2],$$
$$g = (17, (1 - y)/4400) \qquad x = 8, \ y \in [0, 2],$$

while homogeneous boundary conditions are enforced on Γ_D.
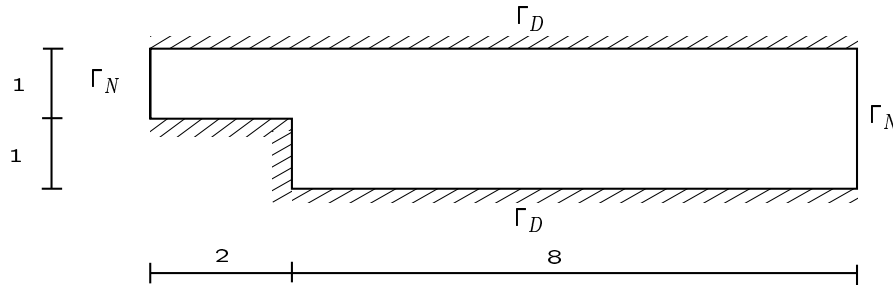
Figure 4. Computational domain and boundary conditions for test case 6.2.

In Fig. 5 we show the refined mesh and a magnified detail around the corner after 15 refinement steps with Algorithm (A). The adaptive mesh is highly refined in correspondence of the areas of strongest stretching and curvature of the flow, in particular around the step corner. In Fig. 6 we show the error estimator $\Phi(\sigma_h; \mathcal{T}_h)$ as a function of N for adaptive and uniform meshes. The convergence rate is slightly more than 1/2 for adaptive meshes and about 2/5 for uniform meshes.
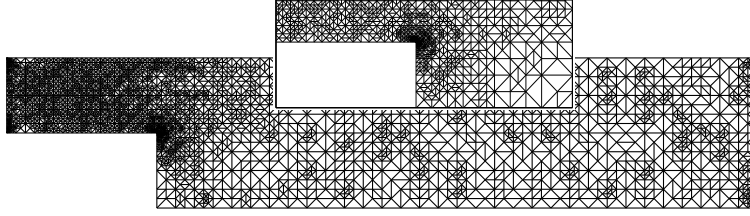
Figure 5. Adapted mesh after 15 iterations of Algorithm (A) and magnified detail around the corner for test case 6.2.
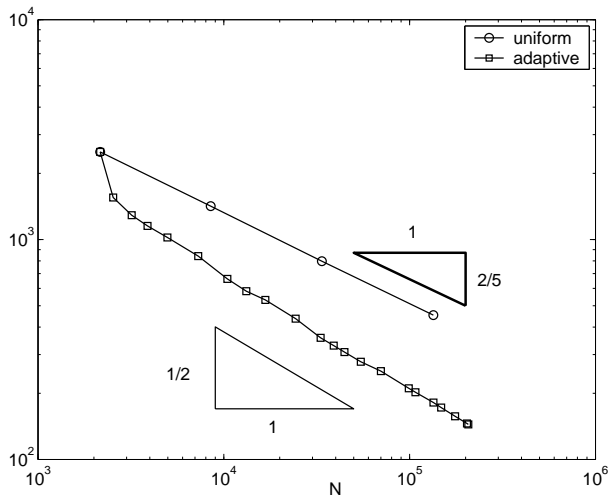
Figure 6. Error estimator as a function of the number of degrees of freedom for uniform and adaptive refinement for test case 6.2.

6.3 L-shaped compressible material domain

We now apply the adaptive refinement algorithm (A) to the numerical solution of the linear elasticity system (5) in both compressible and quasi incompressible regimes. With this aim, we consider an L-shaped domain as in Fig. 7. The radial and tangential components of the exact solution

expressed as functions of the polar coordinates (r, θ) read

$$u_r(r, \theta) = \frac{r^\alpha}{2\mu}(-(\alpha + 1)\cos((\alpha + 1)\theta) + (C_2 - (\alpha + 1))C_1\cos((\alpha - 1)\theta)),$$

$$u_\theta(r, \theta) = \frac{r^\alpha}{2\mu}((\alpha + 1)\sin((\alpha + 1)\theta) + (C_2 + \alpha - 1)C_1\sin((\alpha - 1)\theta)),$$

$$(21)$$

where α is the same value as in test case 6.1, $\omega = 3\pi/4$ and

$$C_1 = -\cos((\alpha + 1)\omega)/\cos((\alpha - 1)\omega), \qquad C_2 = 2(\lambda + 2\mu)/(\lambda + \mu).$$

The Young modulus is $E = 100000$ and numerical computations have been performed with the Poisson ratio ν ranging in the interval

$$\nu = [0.3, 0.45, 0.49, 0.499, 0.4999, 0.49999],$$

the latter value corresponding to a quasi-incompressible problem. Mixed Dirichlet-Neumann boundary conditions are computed from the exact solution and enforced as shown in Fig. 7.
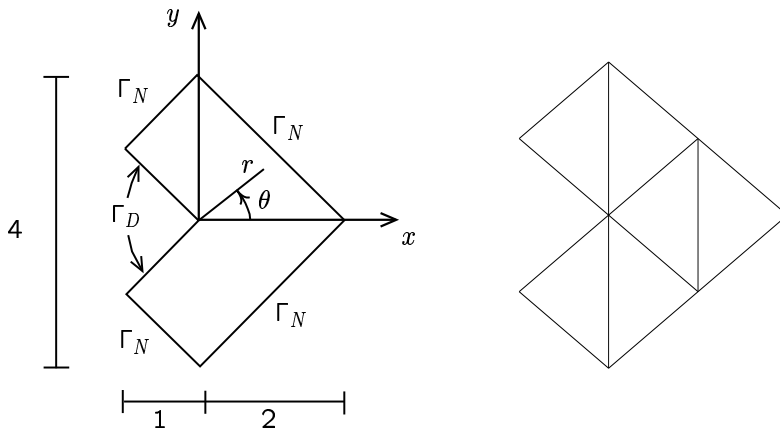
Figure 7. Computational domain (left) and initial mesh (right) for test case 6.3.

In Tab. 3 and Tab. 4 the errors and rates of convergence are displayed for $\nu = 0.3$ and $\nu = 0.49999$, respectively. The experimental convergence rate tends to the value α, as theoretically expected for solutions like (21)(see [19]). The quotient $\frac{|||\sigma - \sigma_h|||}{\Phi(\sigma_h; \mathcal{T}_h)}$ is seen to be bounded from above and below. In Fig. 8 and Tab. 5 we summarize the results of the computation with Algorithm (A). The final mesh after 20 refinement steps is shown in Fig. 9 (left) with von Mises stresses (right). A very strong refinement is produced by the algorithm around the re-entrant corner.

N	h	$\lvert\lvert\lvert\sigma - \sigma_h\rvert\rvert\rvert$	CR	$\lvert\lvert u - u_h\rvert\rvert_{2,\Omega}$	CR	$\frac{\lvert\lvert\lvert\sigma-\sigma_h\rvert\rvert\rvert}{\Phi(\sigma_h;\mathcal{T}_h)}$
100	1.4142	2.247e-02	-	6.487e-04	-	42.719
373	0.7071	9.512e-03	1.240	9.341e-05	2.796	71.241
1441	0.3535	6.015e-03	0.661	2.958e-05	1.658	86.312
5665	0.1768	4.051e-03	0.570	1.338e-05	1.144	89.924
22465	0.0884	2.758e-03	0.554	6.651e-06	1.008	90.986
89473	0.0442	1.884e-03	0.549	3.465e-06	0.940	91.538

Table 3. Error and convergence rates on uniform meshes for test case 6.3 with $\nu = 0.3$.

N	h	$\lvert\lvert\lvert\sigma - \sigma_h\rvert\rvert\rvert$	CR	$\lvert\lvert u - u_h\rvert\rvert_{0,\Omega}$	CR	$\frac{\lvert\lvert\lvert\sigma-\sigma_h\rvert\rvert\rvert}{\Phi(\sigma_h;\mathcal{T}_h)}$
100	1.4142	2.413e-02	-	7.797e-04	-	40.191
373	0.7071	1.014e-02	1.250	9.371e-05	3.056	77.237
1441	0.3535	6.358e-03	0.674	2.869e-05	1.707	99.195
5665	0.1768	4.269e-03	0.574	1.263e-05	1.182	104.213
22465	0.0884	2.904e-03	0.555	6.114e-06	1.047	105.636
89473	0.0442	1.983e-03	0.550	3.112e-06	0.974	106.359

Table 4. Error and convergence rates on uniform meshes for test case 6.3 with $\nu = 0.49999$.
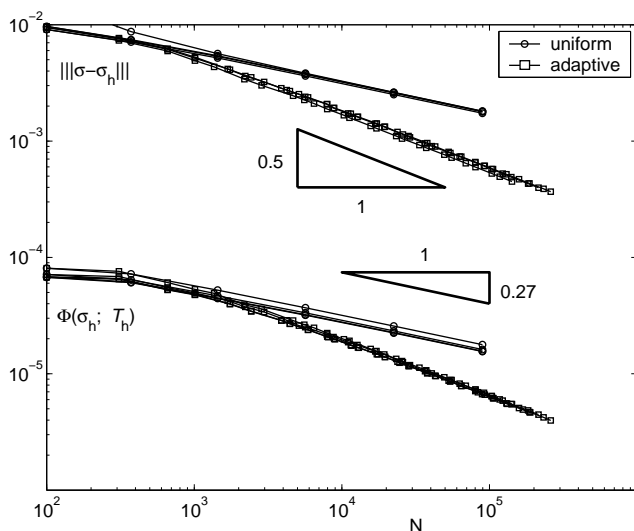

Figure 8. Error and error estimator for uniform and adaptive mesh refinement for test case 6.3 with $\nu = [0.3, 0.45, 0.49, 0.499, 0.4999, 0.49999]$.

6.4 Plate with a hole under traction

As a final test case, we consider a plate with a circular hole, subject to a shearing load on the right side (see Fig. 10, left).

N	h	η_{curl}	CR	η_{As}	CR	η_E	CR
100	1.414214	3.229e-04	-	8.181e-05	-	4.066e-04	-
373	0.707107	7.228e-05	2.159	3.254e-05	1.330	1.073e-04	1.920
1441	0.353553	3.351e-05	1.108	2.004e-05	0.699	5.770e-05	0.896
5665	0.176777	2.105e-05	0.670	1.325e-05	0.596	3.755e-05	0.619
22465	0.088388	1.406e-05	0.581	8.923e-06	0.570	2.531e-05	0.568
89473	0.044194	9.518e-06	0.563	6.063e-06	0.557	1.720e-05	0.557

Table 5. Individual contributions to the error estimator on uniform meshes for test case 6.3 with $\nu = 0.3$.
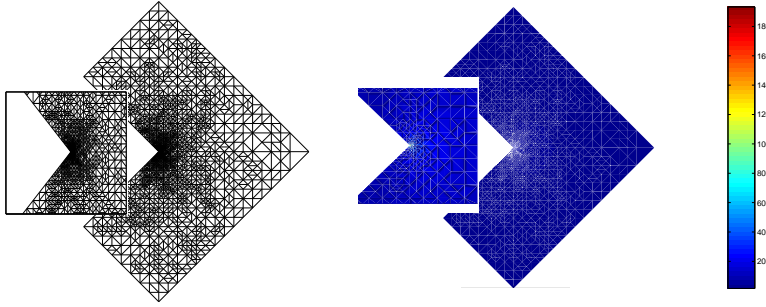
Figure 9. Adapted mesh (left) with a magnified detail of the re-entrant corner and von-Mises stresses (right) with a magnified detail of the re-entrant corner after 20 refinement steps with Algorithm (A) with $\nu = 0.3$ for test case 6.3.

A closed-form solution to the linear elasticity system exists in the case of an infinitely large, thin plate with a circular hole, and the stress normal to the vertical plane of symmetry (y-axis) is

$$\sigma_{xx}|_{x=0} = \begin{cases} \sigma_0 \left(1 + \dfrac{R}{2y^2}\right) & y \geq R, \\ 0 & y < R. \end{cases} \tag{22}$$

We set $\sigma_0 = 1$, $E = 100\,000$ and $\nu = 0.3$. Symmetry boundary conditions are enforced on the boundaries converging to the curved part (that is, on the axis of symmetry of the entire plate, of which Fig. 10 represents the quarter that we study), while Neumann boundary conditions are enforced elsewhere. From (22) we have that at location P of Fig. 10, $\sigma_{xx} = 3\sigma_0$. Since point P is a node, we display the value of σ_{xx} computed by an averaged stress approximation. Observe the significantly better result obtained with the adaptive approximation. In Fig. 11 we plot the value σ_{xx} at P computed using both uniform and adapted meshes. In Fig. 12 (left) we plot the adapted mesh after 15 refinement steps with Algorithm (A) and in Fig. 12
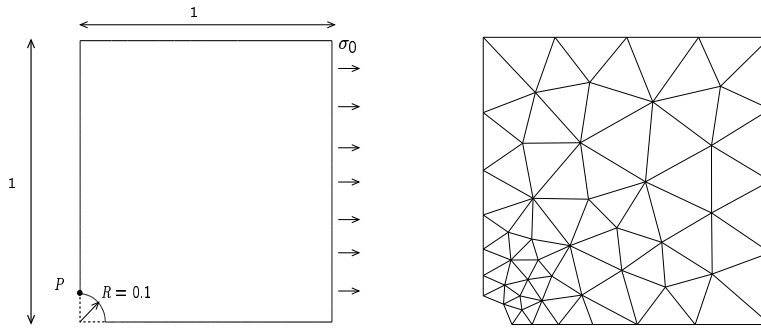
Figure 10. Computational domain (left) and initial mesh (right) for test case 6.4

(right) we plot the corresponding von Mises stresses. We observe that the Algorithm (A) generates a refinement towards the hole, where the stress gradients are higher. The results are independent of the Poisson ratio ν.
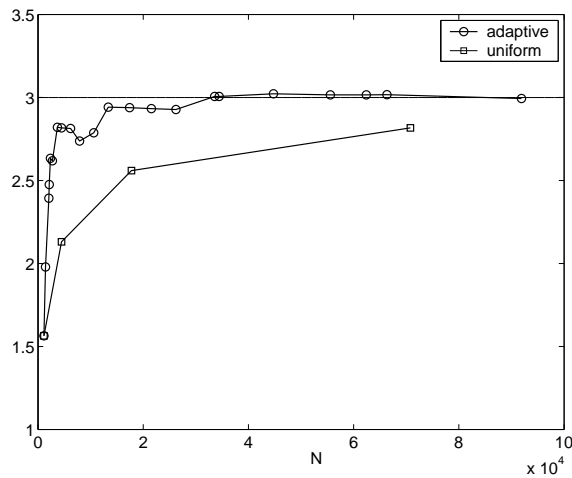
Figure 11. σ_{xx} component of the stress tensor at P as a function of the number of degrees of freedom for test case 6.4 using uniform and adaptive refinement.
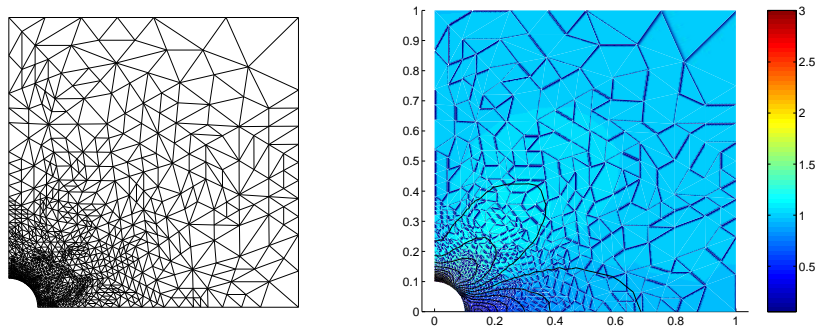
Figure 12. Adapted mesh (left) and von Mises stresses (right) after 15 refinement steps with Algorithm (A) for test case 6.4.

References

1. D.N. Arnold and F. Brezzi. Mixed and nonconforming finite element methods: Implementation, postprocessing and error estimates. *Math. Modeling and Numer. Anal.*, 19-1:7–32, 1985.
2. D.N. Arnold, F. Brezzi, and J. Douglas. PEERS: A new mixed finite element for plane elasticity. *Japan J. Appl. Math.*, 1:347–367, 1984.
3. D.N. Arnold and R. Falk. A new mixed formulation for elasticity. *Numer. Math.*, 53:13–30, 1988.
4. R.E. Bank and B.D. Welfert. A posteriori error estimates for the Stokes problem. *SIAM J. Numer. Anal.*, 28:591–623, 1991.
5. D. Braess. *Finite Elements*. Cambridge University Press, Cambridge, 2001.
6. D. Braess, C. Carstensen, and B.D. Reddy. Uniform convergence and a posteriori error estimators for the enhanced strain. *Numer. Math.*, 96:461–479, 2004.
7. S. Brenner and C. Carstensen. Finite element methods. *Encyclopedia of Computational Mechanics*, 2004 (in press).
8. F. Brezzi and M. Fortin. *Mixed and Hybrid Finite Element Methods*. Springer Verlag, New York, 1991.
9. C. Carstensen. A Unifying Theory of A Posteriori Finite Element Error Control. 2004 (in preparation).
10. C. Carstensen and G. Dolzmann. A posteriori error estimates for mixed FEM in elasticity. *Numer. Math.*, 81:187–209, 1998.
11. C. Carstensen, G. Dolzmann, S.A. Funken, and D.S. Helm. Locking-free adaptive mixed finite element methods in linear elasticity. *Comput. Methods Appl. Mech. Engrg.*, 190:1701–1718, 2000.
12. C. Carstensen and S. Funken. Averaging technique for FE-a posteriori error control in elasticity. Part I: Conforming Fem, part II: λ-independent estimates, part III: Locking-free nonconforming fem. *Comput. Methods Appl. Mech. Engrg*, 190:2483–2498, 2001.

13. C. Carstensen and S. Funken. A posteriori error control in low order finite element discretizations of incompressible stationary flow problems. *Math. Comp.*, 70-236:1353–1381, 2001.

14. P. Causin. *Mixed-hybrid Galerkin and Petrov-Galerkin finite element formulations in fluid mechanics*. PhD thesis, Università degli Studi di Milano, 2002.

15. P. Causin and R. Sacco. A dual-mixed hybrid formulation for fluid mechanics problems: Mathematical analysis and application to semiconductor process technology. *Comput. Methods Appl. Mech. Engrg.*, 192:593–612, 2003.

16. P.G. Ciarlet. *The Finite Element Method for Elliptic Problems*. North Holland, Amsterdam, 1978.

17. K. Eriksson, D. Estep, P. Hansbo, and C. Johnson. Introduction to adaptive methods for differential equations. *Acta Numerica*, pages 105–158, 1995.

18. M. Farhloul and M. Fortin. Dual hybrid methods for the elasticity and the Stokes problems: a unified approach. *Numer. Math.*, 76-4:419–440, 1997.

19. P. Griesvard. Singularities in elasticity theory. In P.G. Ciarlet and E. Sanchez-Palencia, editors, *Applications of multiple scaling in Mechanics*, pages 134–150. Masson, Paris, 1987.

20. L.R. Herrmann. Elasticity equations for incompressible and nearly-incompressible materials by a variational theorem. *AIAA Jnl.*, 3-10:1896–1900, 1965.

21. T.J.R. Hughes. *The Finite Element Method, Linear Static and Dynamic Analysis*. Prentice-Hall, Englewood Cliffs, New Jersey, 1987.

22. P.A. Raviart and J.M. Thomas. A mixed finite element method for second order elliptic problems. In I. Galligani and E. Magenes, editors, *Mathematical Aspects of Finite Element Methods,I*. Springer-Verlag, Berlin, 1977.

23. R. Verfürth. A posteriori error estimator for the Stokes equations. *Numer.Math.*, 55:309–325, 1989.

24. R. Verfürth. A posteriori error estimator for the Stokes equations. II: Nonconforming discretizations. *Numer.Math.*, 60:235–249, 1991.